Supporting Information

Alkyl-Parity Controlled Switching of Polar/Antipolar Organic Semiconductors

Satoru Inoue[a]*, Toshiki Higashino[b], Kiyoshi Nikaido[a], Ryo Miyata[a], Satoshi Matsuoka[a], MutsuoTanaka[c], Seiji Tsuzuki[a], Sachio Horiuchi[b], Ryusuke Kondo[d], Ryoko Sagayama[e], Reiji Kumai[e], Tatsuo Hasegawa[a]*

[a] Department of Applied Physics, The University of Tokyo, 7-3-1 Hongo, Tokyo 113-8656, Japan

[b] Research Institute for Advanced Electronics and Photonics (RIAEP), National Institute of Advanced Industrial Science and Technology (AIST), Tsukuba, Ibaraki 305-8565, Japan

[c] Department of Life Science & Green Chemistry, Saitama Institute of Technology, 1690, Fusaiji, Fukaya, Saitama 369-0293, Japan

[d] Department of Physics, Okayama University, Okayama 700-8530, Japan

[e] Photon Factory, Institute of Materials Structure Science, High Energy Accelerator Research Organization (KEK), Tsukuba, Ibaraki 305-0801, Japan

Materials Synthesis

All chemicals and solvents are of reagent grade unless otherwise indicated. Nuclear magnetic resonance (NMR) spectra were recorded on a JEOL JNM-ECS400 spectrometer at 400MHz. Chemical shifts (δ) are reported in ppm relative to tetramethylsilane (δ 0.00). The data of multiplicity are shown as follows: s = singlet, d = doublet, t = triplet, q = qualtet, m = multiplet. Mass analyses (MS) were performed on a Shimadzu GC-MS QP2010SE in an electron impact ionization procedure. Elemental analyses were collected on a J-Science Lab JM10. As shown in Scheme S1, *p*Tol-BTBT-C$_n$ were all synthesized using Suzuki coupling reaction between Br-BTBT-C$_n$ and *para*-tolylboronic acid. Corresponding Br-BTBT-C$_n$ were synthesized by the reported procedure[S15].

General procedure for the synthesis of *p*Tol-BTBT-C$_n$: A mixture of corresponding Br-BTBT-C$_n$ (1 mmol), *p*-tolylboronic acid (272 mg, 2 mmol, 2.0 eq), K_2CO_3 (276 mg, 5.0 eq), and $Pd(PPh_3)_4$ (57.8 mg, 5 mol%) in a mixed solution of toluene (50 mL) and H_2O (10 mL) was stirred for 5 h at 90 ºC. The organic layer was separated and passed through a silica gel pad with hexane-chloroform (5:1 v/v) as eluent. Purification of the white powdered product obtained by evaporation was finally carried out by recrystallization from a mixed solution of chloroform and ethanol to afford the corresponding *p*Tol-BTBT-C$_n$ as white crystals.

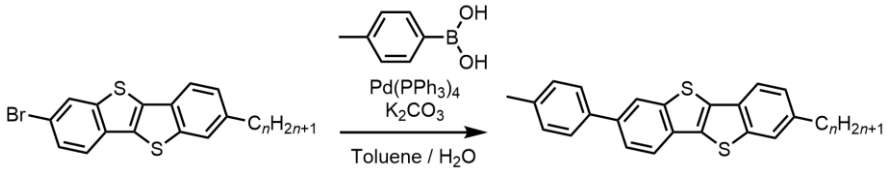

Scheme S1. Synthetic scheme of *p*Tol-BTBT-C$_n$.

***p*Tol-BTBT-C$_5$**: 87 % yield. ^{1}H NMR (400 MHz, $CDCl_3$): δ (ppm) 8.10 (s, 1H, ArH), 7.90 (d, *J* = 8.0 Hz, 1H, ArH), 7.79 (d, *J* = 8.0 Hz, 1H, ArH), 7.73 (s, 1H, ArH), 7.68 (dd, *J* = 8.0, 2.0 Hz, 1H, ArH), 7.59 (d, *J* = 8.0 Hz, 2H, ArH), 7.29 (m, 3H, ArH), 2.77 (t, *J* = 8.0 Hz, 2H, CH_2), 2.42 (s, 3H, $ArCH_3$), 1.71 (tt, *J* = 8.0, 7.2 Hz, 2H, CH_2), 1.37 (m, 4H, CH_2), 0.91 (t, *J* = 7.2 Hz, 3H, CH_3). ^{13}C NMR (100MHz, $CDCl_3$); δ (ppm) 142.90, 142.64, 140.37, 138.05, 137.89, 137.25, 133.53, 132.40, 132.14, 131.09, 129.64, 127.13, 125.93, 124.28, 123.37, 122.04, 121.53, 121.22, 36.11, 31.50, 31.39, 22.57, 21.13, 14.04. MS (EI mode) m/z 400. Anal. Calcd for $C_{26}H_{24}S_2$: C, 77.95%, H, 6.04%. Found: C, 78.03%, H, 6.29%.

***p*Tol-BTBT-C$_6$**: 82 % yield. ^{1}H NMR (400 MHz, $CDCl_3$): δ (ppm) 8.10 (s, 1H, ArH), 7.90 (d, *J* = 8.0 Hz, 1H, ArH), 7.79 (d, *J* = 8.0 Hz, 1H, ArH), 7.73 (s, 1H, ArH), 7.68 (dd, *J* = 8.0, 2.0 Hz, 1H, ArH), 7.59 (d, *J* = 8.0 Hz, 2H, ArH), 7.29 (m, 3H, ArH), 2.77 (t, *J* = 8.0 Hz, 2H, CH_2), 2.42 (s, 3H, $ArCH_3$), 1.71 (tt, *J* = 8.0, 7.2 Hz, 2H, CH_2), 1.33 (m, 6H, CH_2), 0.90 (t, *J* = 7.2 Hz, 3H, CH_3). ^{13}C NMR (100MHz, $CDCl_3$); δ (ppm) 142.90, 142.64, 140.39, 138.06, 137.90, 137.26, 133.53, 132.41, 132.15, 131.10, 129.65, 127.14,

125.94, 124.30, 123.37, 122.05, 121.54, 121.22, 36.16, 31.75, 31.68, 29.00, 22.63, 21.14, 14.11. MS (EI mode) m/z 414. Anal. Calcd for $C_{27}H_{26}S_2$: C, 78.21%, H, 6.32%. Found: C, 78.20%, H, 6.53%.

***p*Tol-BTBT-C$_7$**: 84 % yield. ^{1}H NMR (400 MHz, $CDCl_3$): δ (ppm) 8.10 (s, 1H, ArH), 7.90 (d, *J* = 8.0 Hz, 1H, ArH), 7.79 (d, *J* = 8.0 Hz, 1H, ArH), 7.73 (s, 1H, ArH), 7.68 (dd, *J* = 8.0, 2.0 Hz, 1H, ArH), 7.59 (d, *J* = 8.0 Hz, 2H, ArH), 7.29 (m, 3H, ArH), 2.77 (t, *J* = 8.0 Hz, 2H, CH_2), 2.42 (s, 3H, $ArCH_3$), 1.71 (tt, *J* = 8.0, 7.2 Hz, 2H, CH_2), 1.35-1.27 (m, 8H, CH_2), 0.89 (t, *J* = 7.2 Hz, 3H, CH_3). ^{13}C NMR (100MHz, $CDCl_3$); δ (ppm) 142.90, 142.64, 140.39, 138.06, 137.90, 137.26, 133.53, 132.41, 132.15, 131.10, 129.65, 127.14, 125.94, 124.30, 123.37, 122.05, 121.54, 121.22, 36.16, 31.83, 31.72, 29.29, 29.20, 22.68, 21.14, 14.11. MS (EI mode) m/z 428.2. Anal. Calcd for $C_{28}H_{28}S_2$: C, 78.46%, H, 6.58%. Found: C, 78.61%, H, 6.80%.

***p*Tol-BTBT-C$_8$**: 75 % yield. ^{1}H NMR (400 MHz, $CDCl_3$): δ (ppm) 8.10 (s, 1H, ArH), 7.90 (d, *J* = 8.0 Hz, 1H, ArH), 7.79 (d, *J* = 8.0 Hz, 1H, ArH), 7.73 (s, 1H, ArH), 7.68 (dd, *J* = 8.0, 2.0 Hz, 1H, ArH), 7.59 (d, *J* = 8.0 Hz, 2H, ArH), 7.29 (m, 3H, ArH), 2.77 (t, *J* = 8.0 Hz, 2H, CH_2), 2.42 (s, 3H, $ArCH_3$), 1.70 (tt, *J* = 8.0, 7.2 Hz, 2H, CH_2), 1.35-1.27 (br, 10H, CH_2), 0.88 (t, *J* = 7.2 Hz, 3H, CH_3). ^{13}C NMR (100MHz, $CDCl_3$); δ (ppm) 142.90, 142.64, 140.39, 138.06, 137.90, 137.26, 133.53, 132.41, 132.15, 131.10, 129.65, 127.14, 125.94, 124.30, 123.37, 122.05, 121.54, 121.22, 36.16, 31.89, 31.72, 29.50, 29.34, 29.27, 22.68, 21.14, 14.12. MS (EI mode) m/z 442. Anal. Calcd for $C_{29}H_{30}S_2$: C, 78.68%, H, 6.83%. Found: C, 78.73%, H, 7.02%.

***p*Tol-BTBT-C$_9$**: 77 % yield. ^{1}H NMR (400 MHz, $CDCl_3$): δ (ppm) 8.10 (s, 1H, ArH), 7.90 (d, *J* = 8.0 Hz, 1H, ArH), 7.79 (d, *J* = 8.0 Hz, 1H, ArH), 7.73 (s, 1H, ArH), 7.68 (dd, *J* = 8.0, 2.0 Hz, 1H, ArH), 7.59 (d, *J* = 8.0 Hz, 2H, ArH), 7.29 (m, 3H, ArH), 2.77 (t, *J* = 8.0 Hz, 2H, CH_2), 2.42 (s, 3H, $ArCH_3$), 1.70 (tt, *J* = 8.0, 7.2 Hz, 2H, CH_2), 1.35-1.27 (br, 12H, CH_2), 0.88 (t, *J* = 7.2 Hz, 3H, CH_3). ^{13}C NMR (100MHz, $CDCl_3$); δ (ppm) 142.90, 142.64, 140.39, 138.06, 137.90, 137.26, 133.53, 132.41, 132.15, 131.10, 129.65, 127.14, 125.94, 124.30, 123.37, 122.05, 121.54, 121.22, 36.17, 31.92, 31.74, 29.59, 29.57, 29.36, 29.36, 22.70, 21.16, 14.14. MS (EI mode) m/z 456. Anal. Calcd for $C_{30}H_{32}S_2$: C, 78.90%, H, 7.06%. Found: C, 78.90%, H, 7.16%.

***p*Tol-BTBT-C$_{10}$**: 64 % yield. ^{1}H NMR (400 MHz, $CDCl_3$): δ (ppm) 8.10 (s, 1H, ArH), 7.90 (d, *J* = 8.0 Hz, 1H, ArH), 7.79 (d, *J* = 8.0 Hz, 1H, ArH), 7.73 (s, 1H, ArH), 7.68 (dd, *J* = 8.0, 2.0 Hz, 1H, ArH), 7.59 (d, *J* = 8.0 Hz, 2H, ArH), 7.29 (m, 3H, ArH), 2.77 (t, *J* = 8.0 Hz, 2H, CH_2), 2.42 (s, 3H, $ArCH_3$), 1.70 (tt, *J* = 8.0, 7.2 Hz, 2H, CH_2), 1.35-1.27 (br, 14H, CH_2), 0.88 (t, *J* = 7.2 Hz, 3H, CH_3). ^{13}C NMR (100MHz, $CDCl_3$); δ (ppm) 142.90, 142.64, 140.39, 138.06, 137.90, 137.26, 133.53, 132.41, 132.15, 131.10, 129.65, 127.14, 125.94, 124.30, 123.37, 122.05, 121.54, 121.22, 36.16, 31.91, 31.71, 29.62, 29.61, 29.53, 29.34(2C), 22.69, 21.14, 14.12. MS (EI mode) m/z 470. Anal. Calcd for $C_{31}H_{34}S_2$: C, 79.10%, H, 7.28%. Found: C, 79.03%, H, 7.30%.

***p*Tol-BTBT-C$_{11}$**: 72 % yield. ^{1}H NMR (400 MHz, $CDCl_3$): δ (ppm) 8.10 (s, 1H, ArH), 7.90 (d, *J* = 8.0 Hz, 1H, ArH), 7.79 (d, *J* = 8.0 Hz, 1H, ArH), 7.73 (s, 1H, ArH), 7.68 (dd, *J* = 8.0, 2.0 Hz, 1H, ArH), 7.59 (d, *J* = 8.0 Hz, 2H, ArH), 7.29 (m, 3H, ArH), 2.77 (t, *J* = 8.0 Hz, 2H, CH_2), 2.42 (s, 3H, $ArCH_3$), 1.70 (tt, *J* = 8.0, 7.2 Hz, 2H, CH_2), 1.35-1.27 (br, 16H, CH_2), 0.88 (t, *J* = 7.2 Hz, 3H, CH_3). ^{13}C NMR (100MHz, $CDCl_3$); δ (ppm) 142.90, 142.64, 140.39, 138.06, 137.90, 137.26, 133.53, 132.41, 132.15, 131.10, 129.65, 127.14, 125.94, 124.30, 123.37, 122.05, 121.54, 121.22, 36.16, 31.92, 31.71, 29.67, 29.63, 29.60, 29.54, 29.35, 29.32, 22.69, 21.14, 14.13. MS (EI mode) m/z 484. Anal. Calcd for $C_{32}H_{36}S_2$: C, 79.29%, H, 7.49%. Found: C, 79.16%, H, 7.51%.

***p*Tol-BTBT-C$_{12}$**: 92 % yield. ^{1}H NMR (400 MHz, $CDCl_3$): δ (ppm) 8.10 (s, 1H, ArH), 7.90 (d, *J* = 8.0 Hz, 1H, ArH), 7.79 (d, *J* = 8.0 Hz, 1H, ArH), 7.73 (s, 1H, ArH), 7.68 (dd, *J* = 8.0, 2.0 Hz, 1H, ArH), 7.59 (d, *J* = 8.0 Hz, 2H, ArH), 7.29 (m, 3H, ArH), 2.77 (t, *J* = 8.0 Hz, 2H, CH_2), 2.42 (s, 3H, $ArCH_3$), 1.70 (tt, *J* = 8.0, 7.2 Hz, 2H, CH_2), 1.35-1.27 (br, 18H, CH_2), 0.88 (t, *J* = 7.2 Hz, 3H, CH_3). ^{13}C NMR (100MHz, $CDCl_3$); δ (ppm) 142.90, 142.64, 140.39, 138.06, 137.90, 137.26, 133.53, 132.41, 132.15, 131.10, 129.65, 127.14, 125.94, 124.30, 123.37, 122.05, 121.54, 121.22, 36.15, 31.93, 31.71, 29.67(3C), 29.60, 29.53, 29.36, 29.31, 22.70, 21.14, 14.13. MS (EI mode) m/z 498. Anal. Calcd for $C_{33}H_{38}S_2$: C, 79.47%, H, 7.68%. Found: C, 79.09%, H, 7.63%.

***p*Tol-BTBT-C$_{13}$**: 59 % yield. ^{1}H NMR (400 MHz, $CDCl_3$): δ (ppm) 8.10 (s, 1H, ArH), 7.90 (d, *J* = 8.0 Hz, 1H, ArH), 7.79 (d, *J* = 8.0 Hz, 1H, ArH), 7.73 (s, 1H, ArH), 7.68 (dd, *J* = 8.0, 2.0 Hz, 1H, ArH), 7.59 (d, *J* = 8.0 Hz, 2H, ArH), 7.29 (m, 3H, ArH), 2.77 (t, *J* = 8.0 Hz, 2H, CH_2), 2.42 (s, 3H, $ArCH_3$), 1.70 (tt, *J* = 8.0, 7.2 Hz, 2H, CH_2), 1.35-1.27 (br, 20H, CH_2), 0.88 (t, *J* = 7.2 Hz, 3H, CH_3). ^{13}C NMR (100MHz, $CDCl_3$); δ (ppm) 142.90, 142.64, 140.39, 138.06, 137.90, 137.26, 133.53, 132.41, 132.15, 131.10, 129.65, 127.14, 125.94, 124.30, 123.37, 122.05, 121.54, 121.22, 36.15, 31.93, 31.71, 29.67(4C), 29.60, 29.53, 29.36, 29.31, 22.70, 21.14, 14.13. MS (EI mode) m/z 512. Anal. Calcd for $C_{34}H_{40}S_2$: C, 79.63%, H, 7.86%. Found: C, 79.53%, H, 7.80%.

***p*Tol-BTBT-C$_{14}$**: 61 % yield. ^{1}H NMR (400 MHz, $CDCl_3$): δ (ppm) 8.10 (s, 1H, ArH), 7.90 (d, *J* = 8.0 Hz, 1H, ArH), 7.79 (d, *J* = 8.0 Hz, 1H, ArH), 7.73 (s, 1H, ArH), 7.68 (dd, *J* = 8.0, 2.0 Hz, 1H, ArH), 7.59 (d, *J* = 8.0 Hz, 2H, ArH), 7.29 (m, 3H, ArH), 2.77 (t, *J* = 8.0 Hz, 2H, CH_2), 2.42 (s, 3H, $ArCH_3$), 1.70 (tt, *J* = 8.0, 7.2 Hz, 2H, CH_2), 1.35-1.27 (br, 22H, CH_2), 0.88 (t, *J* = 7.2 Hz, 3H, CH_3). ^{13}C NMR (100MHz, $CDCl_3$); δ (ppm) 142.90, 142.64, 140.39, 138.06, 137.90, 137.26, 133.53, 132.41, 132.15, 131.10, 129.65, 127.14, 125.94, 124.30, 123.37, 122.05, 121.54, 121.22, 36.15, 31.93, 31.71, 29.67(5C), 29.60, 29.53, 29.37, 29.31, 22.70, 21.11, 14.13. MS (EI mode) m/z 526. Anal. Calcd for $C_{35}H_{42}S_2$: C, 79.79%, H, 8.04%. Found: C, 79.35%, H, 7.75%.

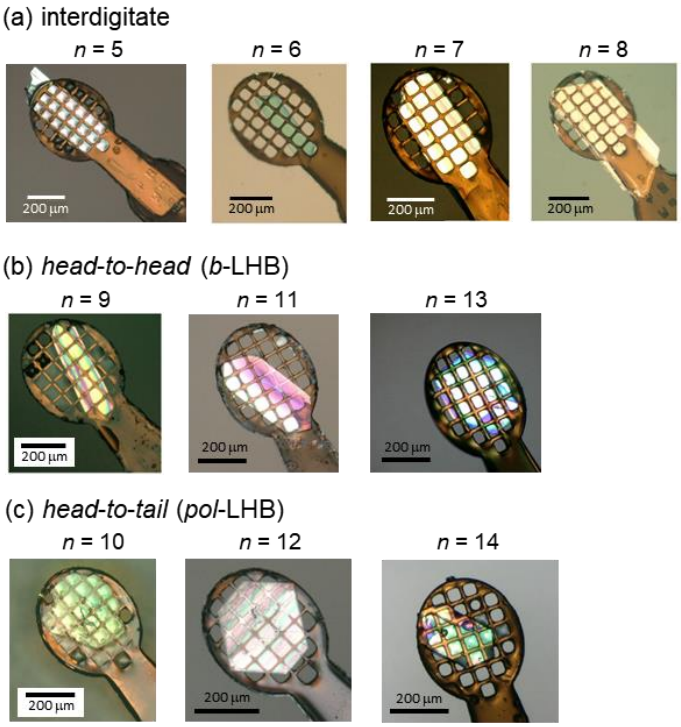

Figure S1. Optical micrographs for single crystals of *p*Tol-BTBT-C$_n$ for crystal structure analyses.

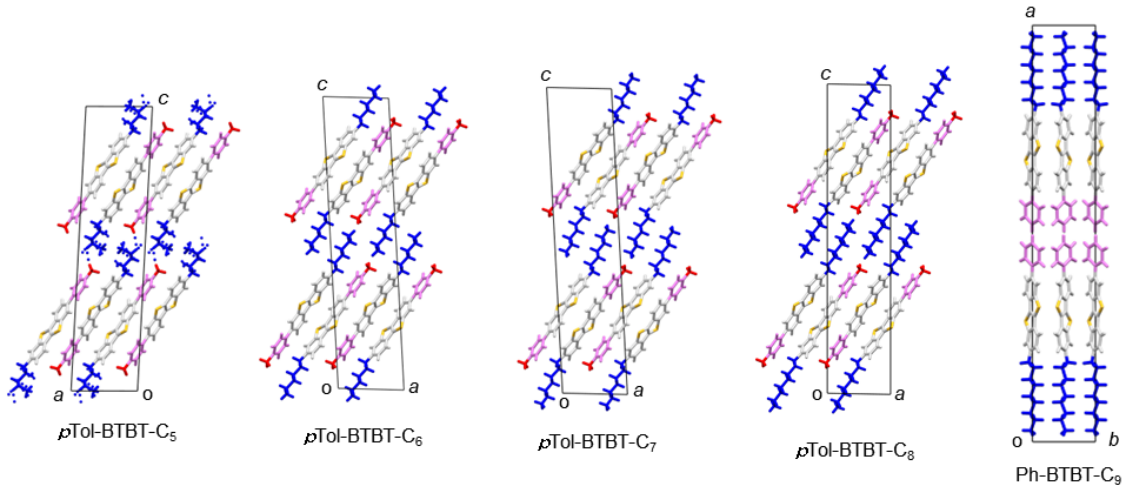

Figure S2. Packing diagrams of *p*Tol-BTBT-C$_n$ (n = 5−8) and Ph-BTBT-C$_9$. Sulfur and carbon atom of the BTBT moiety are shown by the color of yellow and white, respectively, whereas alkyl chains, phenyl groups, and end methyl groups by blue, pink, and red.

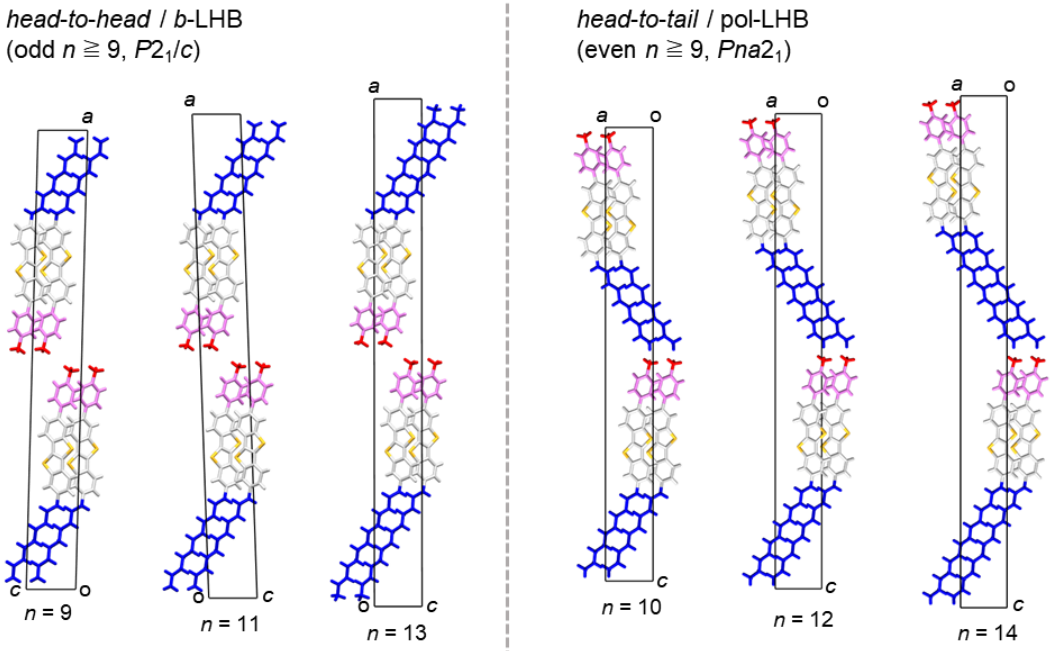

Figure S3. Packing diagrams of *p*Tol-BTBT-C$_n$ (n = 9−14) projected along the *a*-*c* plane. Sulfur and carbon atoms of the BTBT moiety are shown by the color of yellow and white, respectively, whereas alkyl chains, phenyl groups, and end methyl groups by blue, pink, and red.

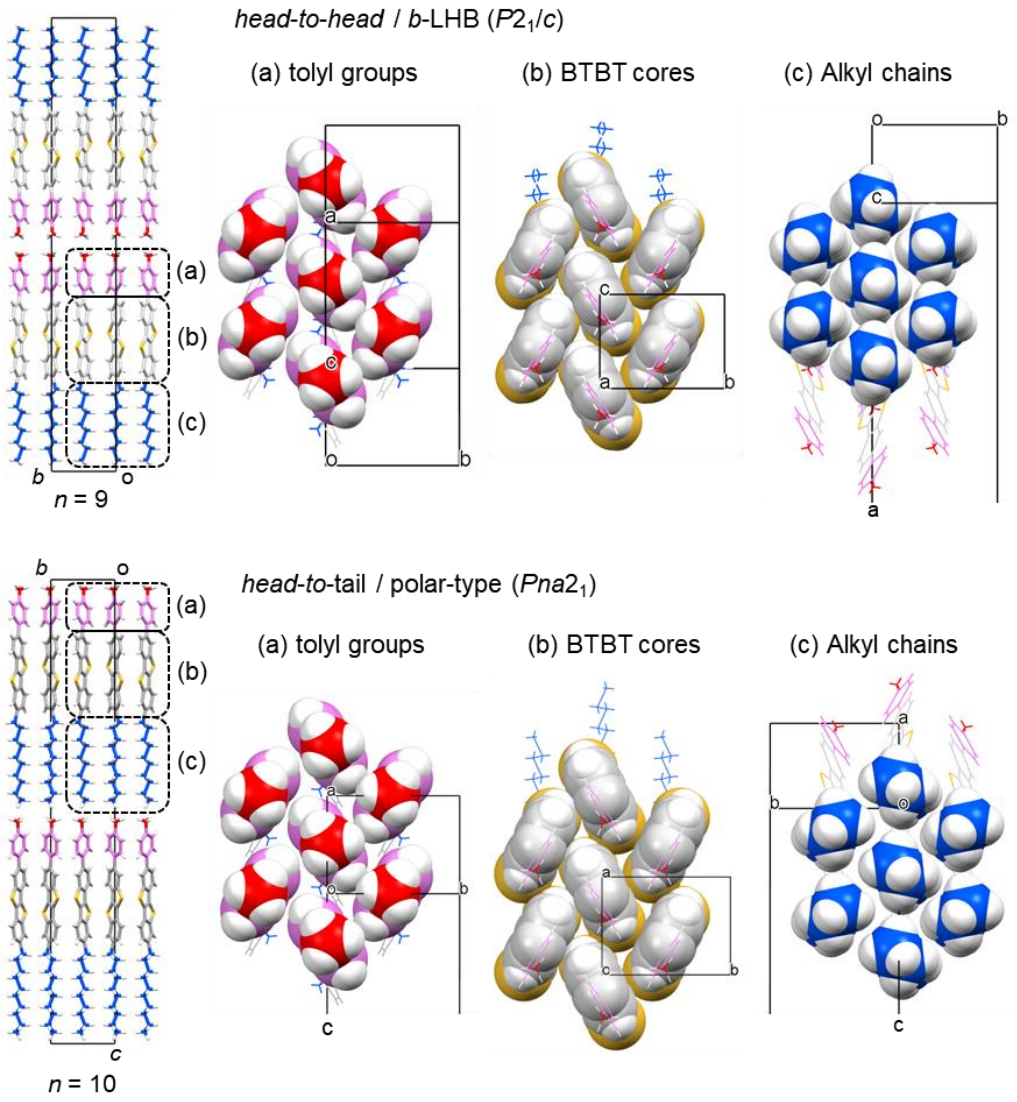

Figure S4. Intermolecular packing arrangement of the *p*Tol-BTBT-C_9 (top) and *p*Tol-BTBT-C_{10} (bottom) depicted by space-filling views for each molecular moiety: (a) *para*-tolyl groups, (b) BTBT cores, and (c) alkyl chains.

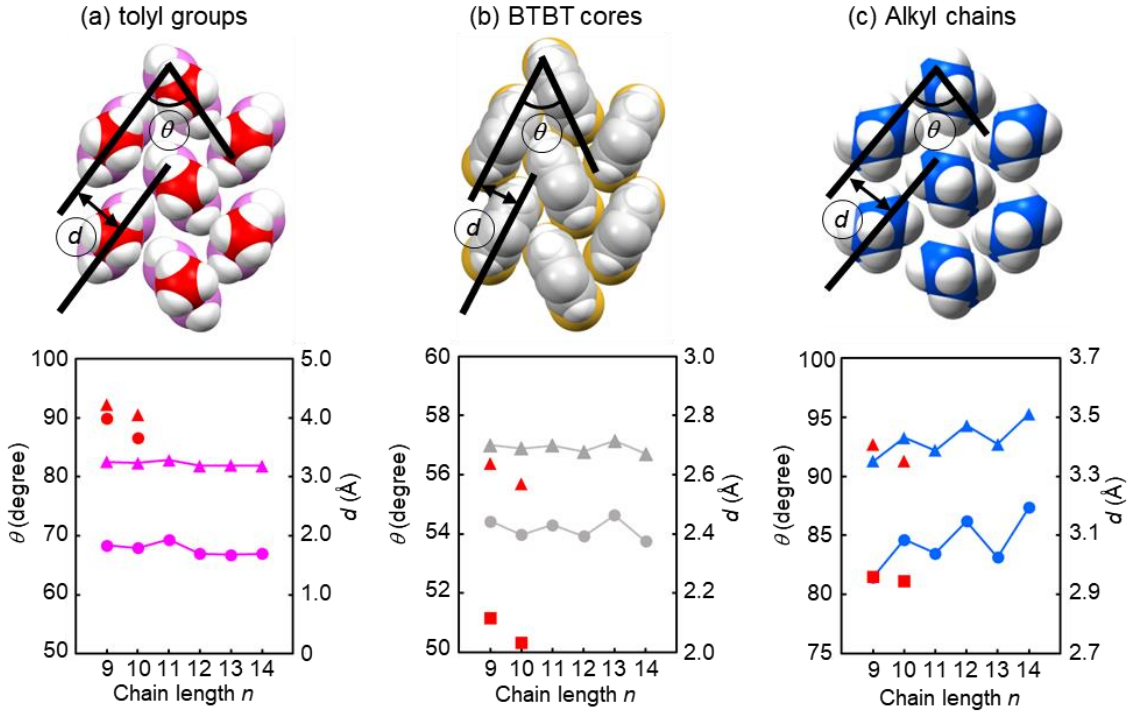

Figure S5. Variation of intralayer molecular packing arrangement in *p*Tol-BTBT-C$_n$ (n = 9–12). The changes in dihedral angles θ(○) and mean interplanar distance d (△) are plotted as a function of alkyl chain length n for the layers of (a) tolyl groups, (b) BTBT cores, and (c) all-trans alkyl chain plane. Definition of the dihedral angles and mean interplanar distances are shown in the corresponding space-filling views. Red plots show the results of Ph-BTBT-C$_n$ (n = 9 and 10).

Table S1. Crystallographic parameters of Ph-BTBT-C_9 and *p*Tol-BTBT-C_n.

Compounds	Ph-BTBT-C_9	*p*Tol-BTBT-C_5	*p*Tol-BTBT-C_6	*p*Tol-BTBT-C_7	*p*Tol-BTBT-C_8
Chemical formula	$C_{29}H_{30}S_2$	$C_{26}H_{24}S_2$	$C_{27}H_{26}S_2$	$C_{28}H_{28}S_2$	$C_{29}H_{30}S_2$
Formula weight	442.68	400.60	414.62	428.65	442.68
Crystal system	monoclinic	monoclinic	monoclinic	monoclinic	monoclinic
Space group	$P2_1/c$	$P2_1/c$	$P2_1/n$	$P2_1/n$	$P2_1/n$
a (Å)	51.657(9)	9.1167(5)	9.1363(5)	9.1572(3)	9.0903(4)
b (Å)	7.8515(14)	5.9715(3)	5.9272(2)	5.9434(2)	5.9152(3)
c (Å)	6.1099(9)	39.007(2)	40.763(2)	43.0458(15)	44.417(2)
α (deg)	90	90	90	90	90
β (deg)	90.843(15)	92.845(5)	94.484(5)	94.237(3)	91.059(4)
γ (deg)	90	90	90	90	90
V (Å^3)	2477.8(7)	2120.94(19)	2200.67(18)	2336.36(14)	2387.94(19)
Z vaule	4	4	4	4	4
Dcalc (g/cm^3)	1.187	1.254	1.251	1.219	1.231
Temperature	300	300	300	300	300
Radiation	MoKα	MoKα	MoKα	MoKα	MoKα
No. of reflections	5742	4864	5014	5264	5346
No. of valuables	280	253	262	271	280
R (I>2σ(I))	0.1558	0.0717	0.0763	0.0744	0.1421
wR^2	0.3614	0.1817	0.1290	0.1721	0.3691

Compounds	*p*Tol-BTBT-C_9	*p*Tol-BTBT-C_{10}	*p*Tol-BTBT-C_{11}	*p*Tol-BTBT-C_{12}	*p*Tol-BTBT-C_{13}	*p*Tol-BTBT-C_{14}
Chemical formula	$C_{30}H_{32}S_2$	$C_{31}H_{34}S_2$	$C_{32}H_{36}S_2$	$C_{33}H_{38}S_2$	$C_{34}H_{40}S_2$	$C_{35}H_{42}S_2$
Formula weight	456.70	470.73	484.78	498.78	512.78	526.84
Crystal system	monoclinic	orthorhombic	monoclinic	orthorhombic	monoclinic	orthorhombic
Space group	$P2_1/c$	$Pna2_1$	$P2_1/c$	$Pna2_1$	$P2_1/c$	$Pna2_1$
a (Å)	54.718(2)	5.92852(18)	59.180(6)	5.90933(13)	63.005(18)	5.9024(5)
b (Å)	7.8060(4)	7.7655(2)	7.8152(8)	7.7398(2)	7.852(3)	7.7178(8)
c (Å)	5.9079(3)	56.2232(16)	5.9147(5)	60.5371(17)	5.9208(16)	64.954(4)
α (deg)	90	90	90	90	90	90
β (deg)	91.482(4)	90	91.9725(16)	90	90.041(6)	90
γ (deg)	90	90	90	90	90	90
V (Å^3)	2522.6(2)	2588.40(13)	2733.9(5)	2768.79(12)	2929.0(15)	2958.9(4)
Z vaule	4	4	4	4	4	4
Dcalc (g/cm^3)	1.202	1.208	1.178	1.196	1.163	1.183
Temperature	300	300	300	300	300	300
Radiation	MoKα	MoKα	synchrotron (λ = 1.000 Å)	MoKα	synchrotron (λ = 1.233 Å)	MoKα
No. of reflections	5772	6583	1879	5425	2501	6673
No. of valuables	289	298	207	316	227	334
R (I>2σ(I))	0.1348	0.0622	0.0908	0.0434	0.1668	0.1016
wR^2	0.2932	0.1234	0.2226	0.0972	0.4660	0.1636

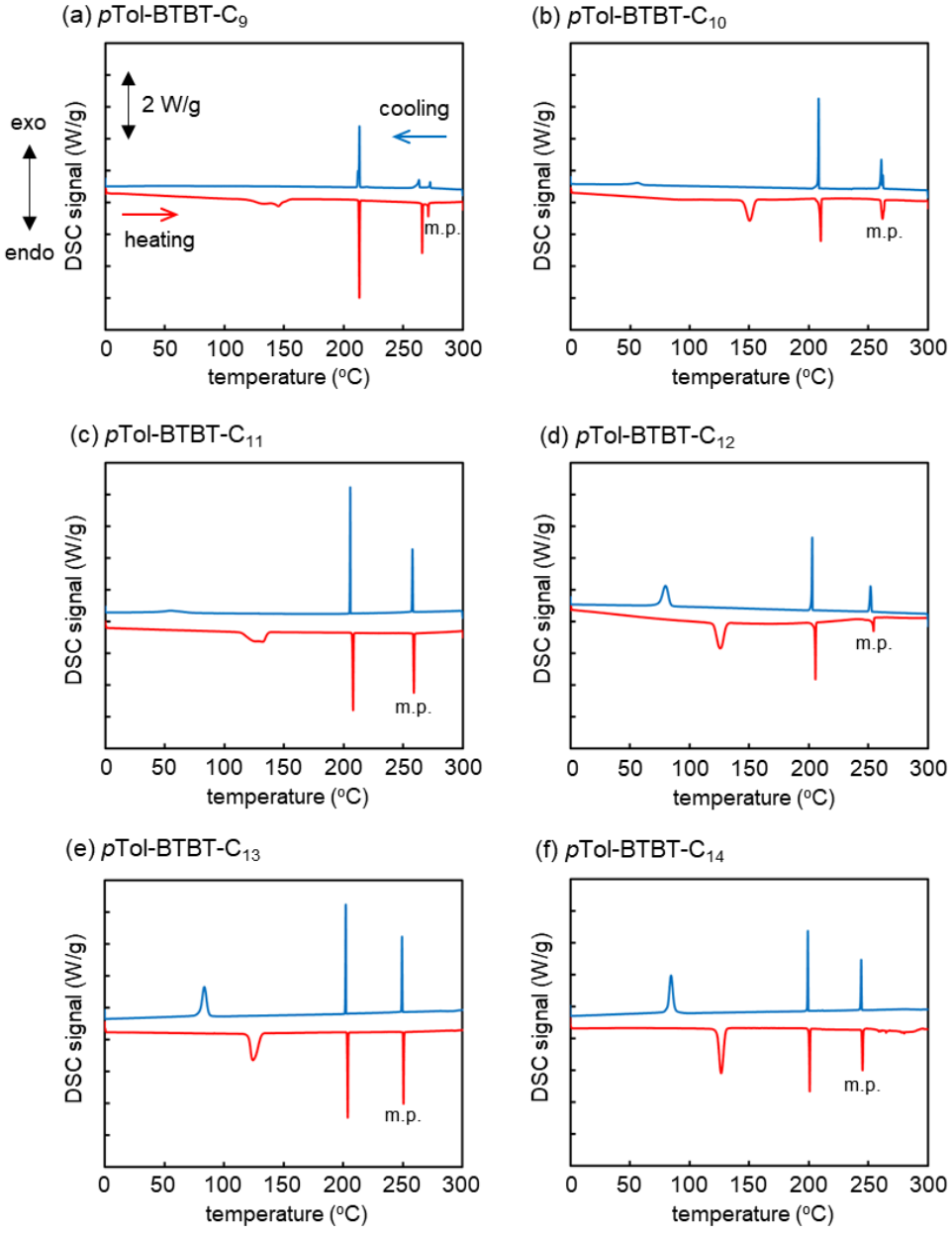

Figure S6. DSC charts of *p*Tol-BTBT-C$_n$ for (a) n = 9, (b) n = 10, (c) n = 11, (d) n = 12, (e) n = 13, and (f) n = 14 measured at 5 K/min. Red curves and blue curves show the results for first heating run and subsequent cooling run, respectively.

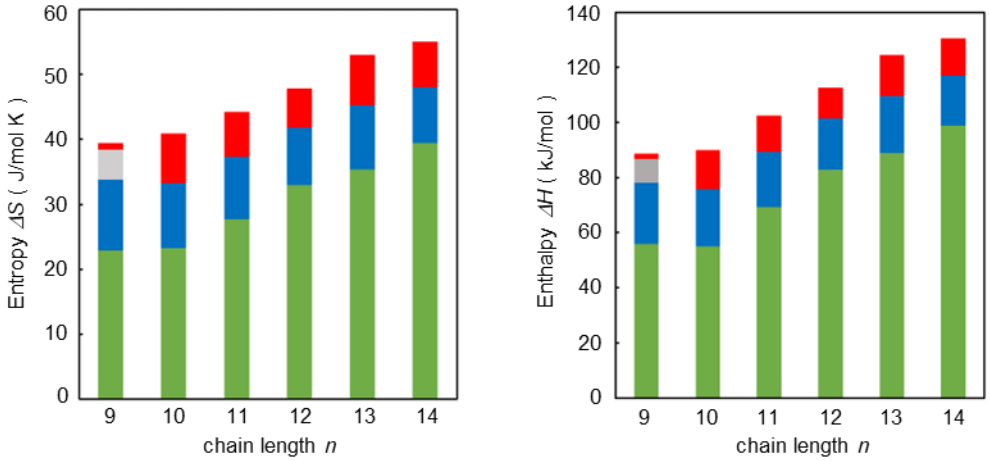

Figure S7. Changes in enthalpy ΔS and entropy ΔH, calculated from DSC charts in the heating step. ΔS: $\Delta H/T_{trans}$, ΔH: enthalpy change, and T_{trans}: phase transition temperature, green: crystal to smectic E phase transition, blue: smectic E to liquid-crystal phase transition, red: melting point, gray: phase transition at 265 °C for n = 9 (where the peak was observed before melting point).

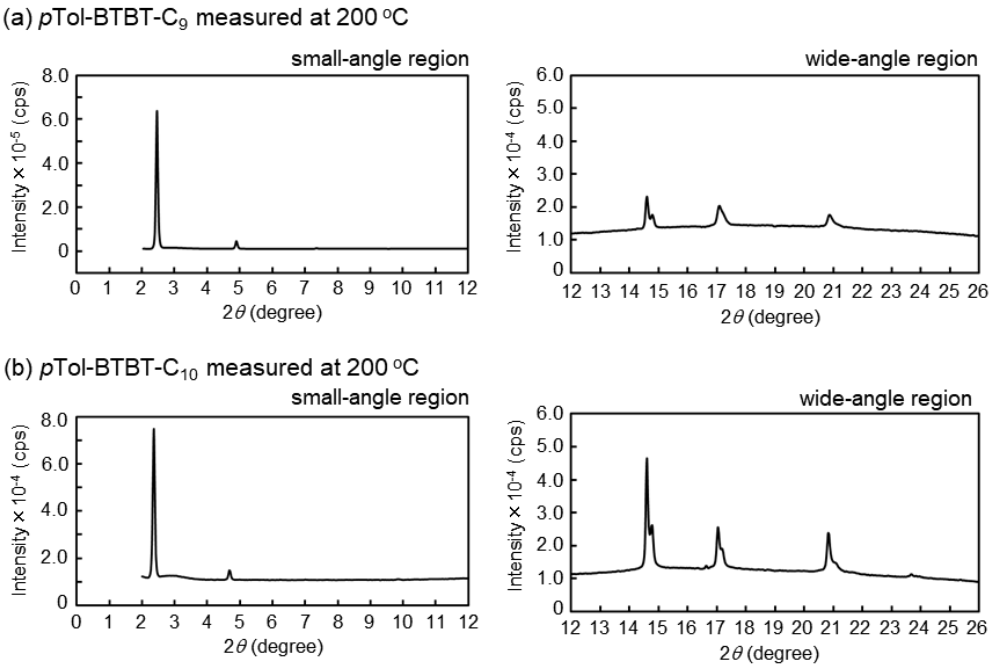

Figure S8. Powder XRD profiles of (a) *p*Tol-BTBT-C_9 and (b) *p*Tol-BTBT-C_{10} measured at 200 °C in the small-angle region (left) and wide-angle region (right).

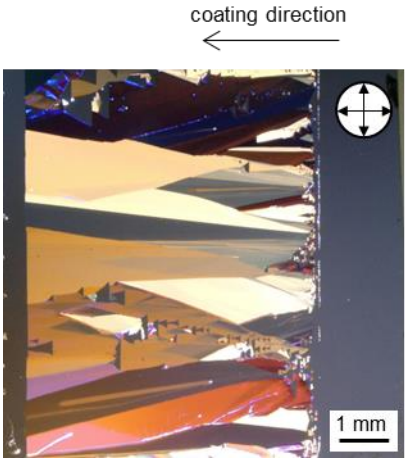

Figure S9. An crossed-Nicols polarized optical microscope image of blade-coated single-crystal thin film of *p*Tol-BTBT-C_{10}. As the film is composed of several single crystal domains, we used a single domain after trimming other crystal domains away for the XRD measurements.

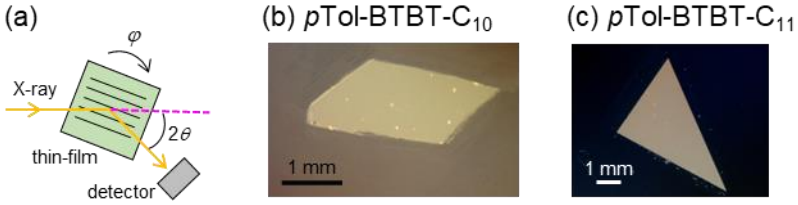

Figure S10. (a) Schematic experimental setup for in-plane XRD measurements of single-crystal films. (b)(c) Crossed-Nicols polarized micrographs for isolated single crystal domain film of *p*Tol-BTBT-C_{10} (thickness: 20 nm) and *p*Tol-BTBT-C_{11} (thickness: 16 nm) used for the XRD measurements.

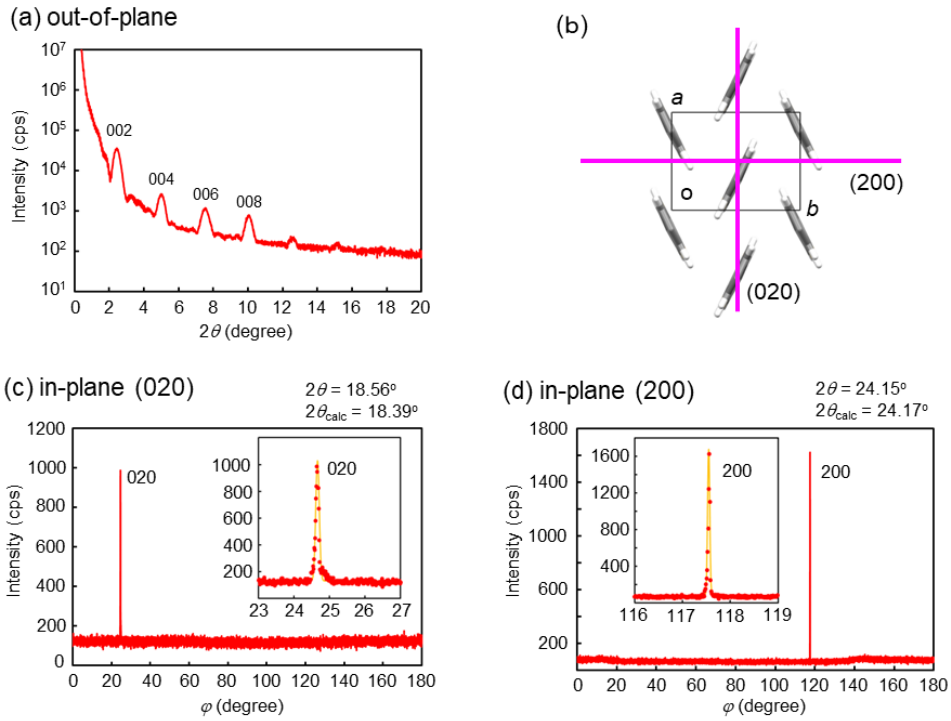

Figure S11. (a) Out-of-plane XRD profiles of the single-crystal thin film of *p*Tol-BTBT-C_{10} shown in Figure S10b. (b) Schematics for the arrangement of BTBT cores in *a*-*b* plane (in-plane) obtained by the crystallographic data of *p*Tol-BTBT-C_{10} bulk crystal. Purple lines show (200) and (020) plane, respectively. (c)(d) In-plane-XRD profiles of the single-crystal thin film of *p*Tol-BTBT-C_{10} shown in Figure S10b. $2\theta_{calc}$ means the value calculated from the crystallographic data of bulk crystal. The used wavelength λ of the synchrotron X-rays was = 1.241 Å.

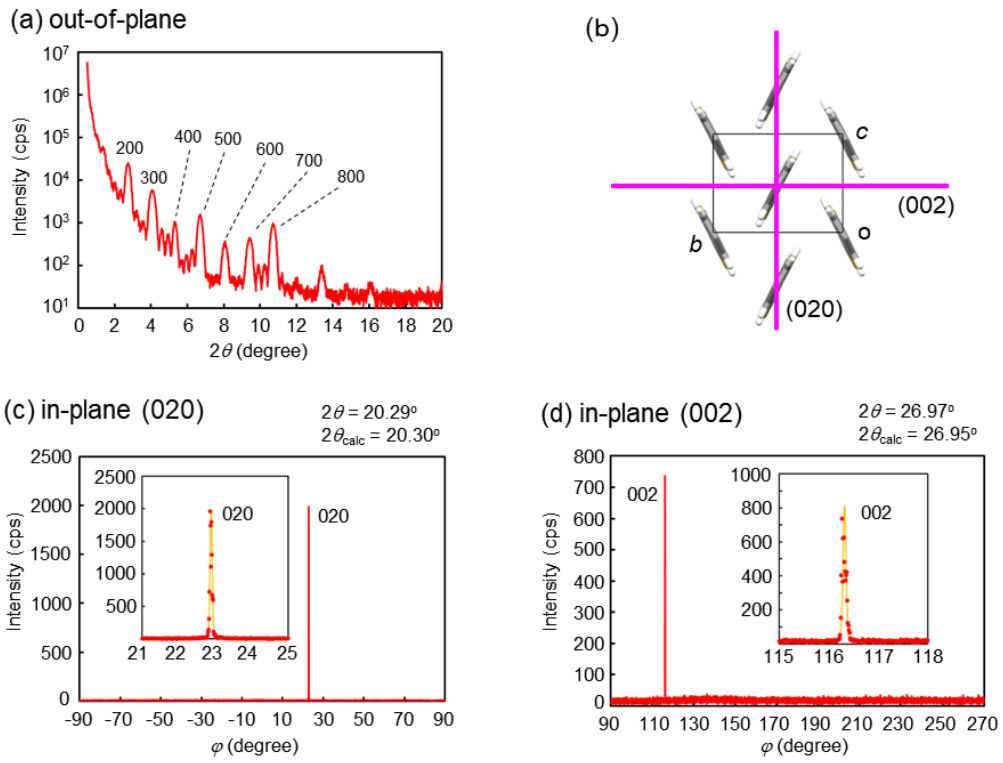

Figure S12. (a) Out-of-plane XRD profiles of the single-crystal thin film of *p*Tol-BTBT-C_{11} shown in Figure S10c. (b) Schematics for the arrangement of BTBT cores in *b*-*c* plane (in-plane) obtained by the crystallographic data of *p*Tol-BTBT-C_{11} bulk crystal. Purple lines show (002) and (020) plane, respectively. (c)(d) In-plane-XRD profiles of the single-crystal thin film of *p*Tol-BTBT-C_{11} shown in Figure S10c. $2\theta_{calc}$ means the value calculated from the crystallographic data of bulk crystal. The used wavelength λ of the synchrotron X-rays was 1.377 Å.

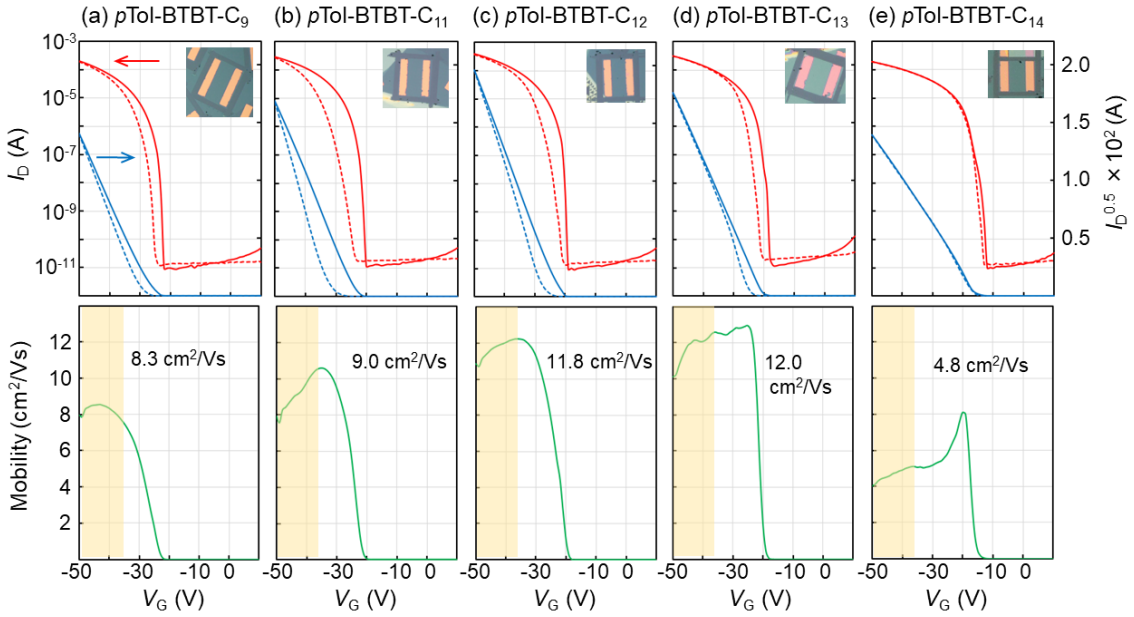

Figure S13. Typical transfer characteristics (top) and V_G-dependent mobility (bottom) of bottom-gate/top-contact (BGTC) OFETs based on (a) *p*Tol-BTBT-C$_9$, (b) *p*Tol-BTBT-C$_{11}$, (c) *p*Tol-BTBT-C$_{12}$, (d) *p*Tol-BTBT-C$_{13}$, and (e) *p*Tol-BTBT-C$_{14}$ single crystals, measured at $V_D = -50$V. Solid and dashed curves exhibit the data at forward and backward scans, respectively. Optical microscope images of the devices are shown in the each inset of the top graph. The mobility values calculated from the average at $V_G = -35 \sim -50$V are shown in the each inset of the bottom graph.

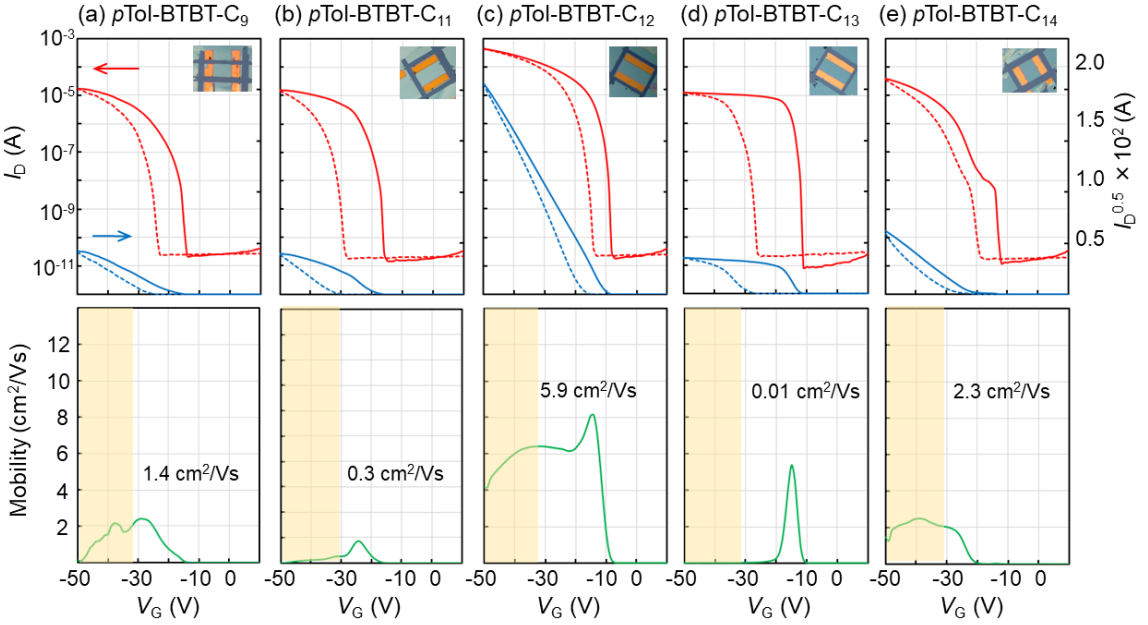

Figure S14. Typical transfer characteristics (top) and V_G-dependent mobility (bottom) of bottom-gate/bottom-contact (BGBC) OFETs based on (a) *p*Tol-BTBT-C_9, (b) *p*Tol-BTBT-C_{11}, (c) *p*Tol-BTBT-C_{12}, (d) *p*Tol-BTBT-C_{13}, and (e) *p*Tol-BTBT-C_{14} single crystals, measured at $V_D = -50$V. Solid and dashed curves exhibit the data at forward and backward scans, respectively. Optical microscope images of the devices are shown in the each inset of the top graph. The mobilities values calculated from the average at $V_G = -30 \sim -50$V are shown in the each inset of the bottom graph.

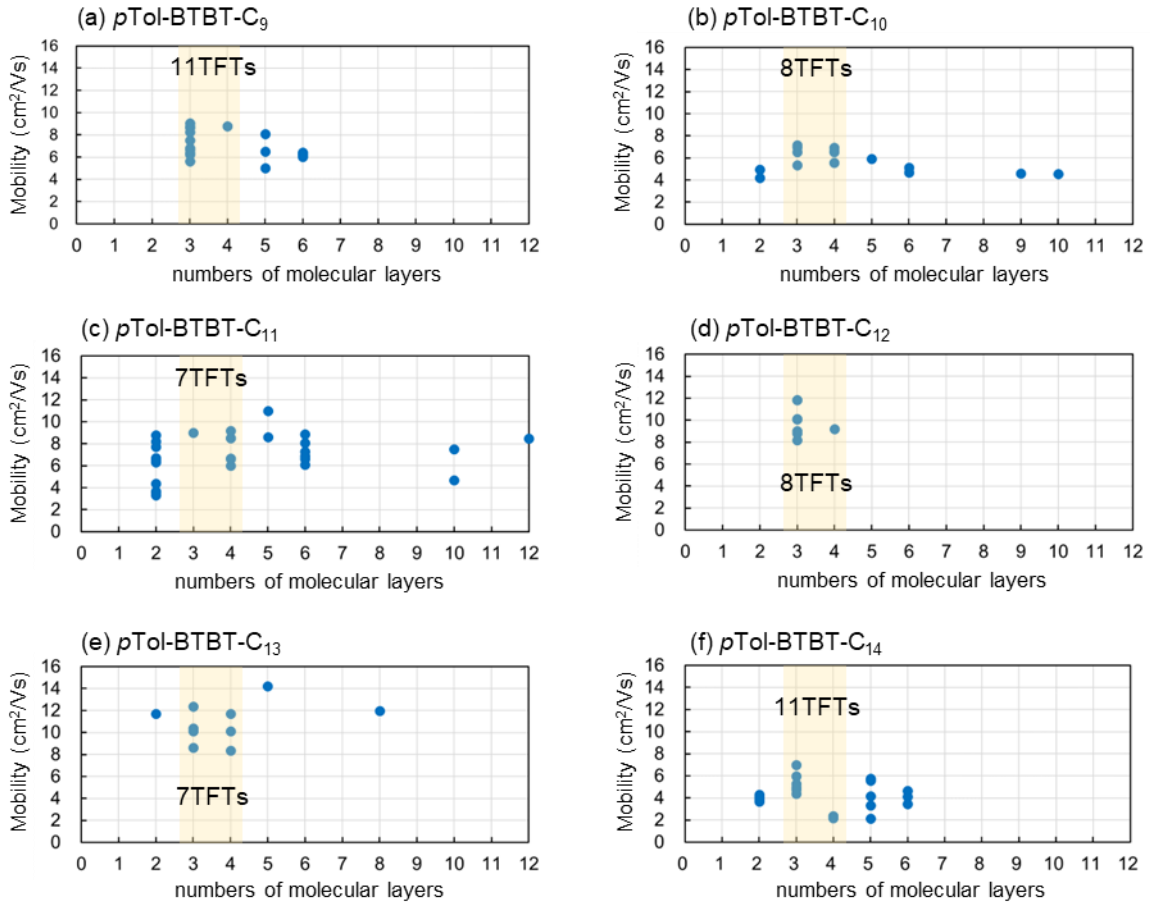

Figure S15. Values of the estimated BGTC device mobility are plotted as a function of the layer number thickness of the films. Average values at each orange area (limiting 3−4-layer thickness) are used in Figure 4c of the main manuscript.

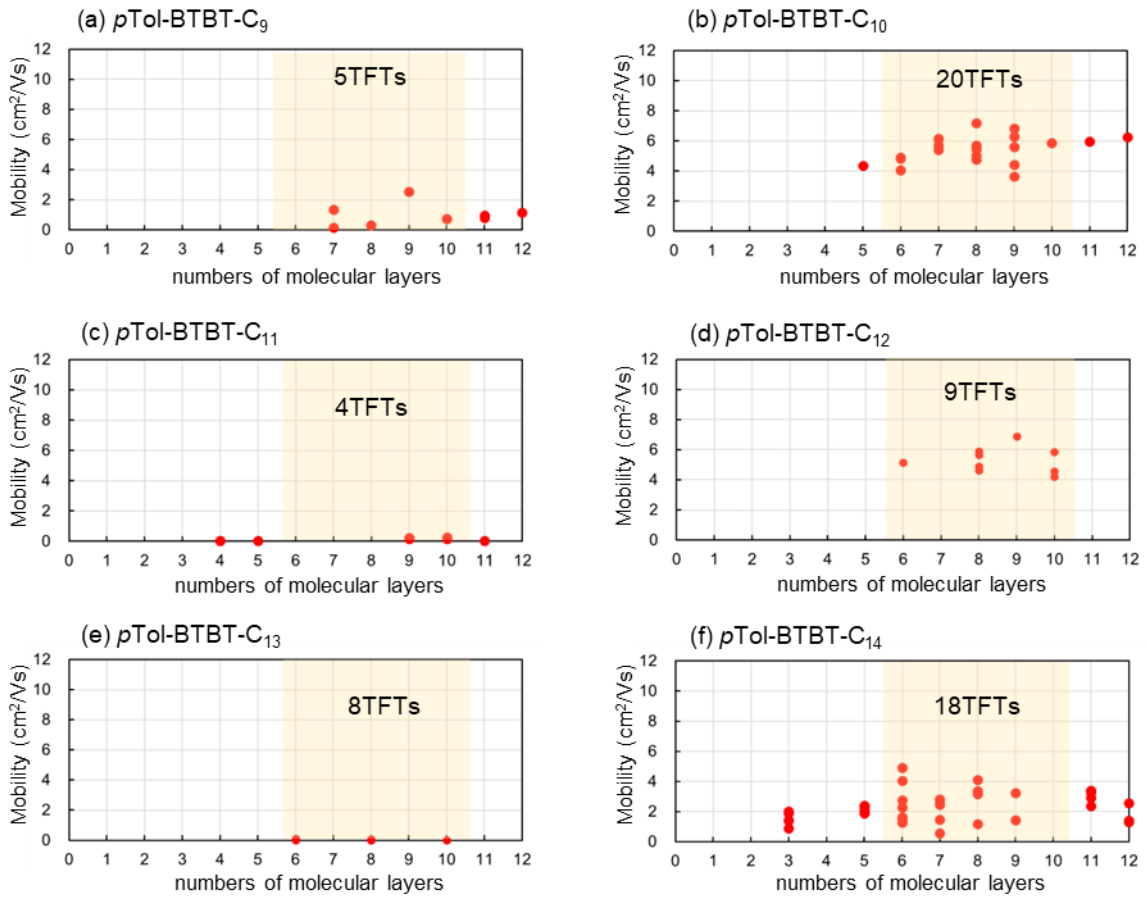

Figure S16. Values of the estimated BGBC device mobility are plotted as a function of the layer number thickness of the films. Average values at each orange area (limiting 6−10-layer thickness) are used in Figure 4c of the main manuscript.

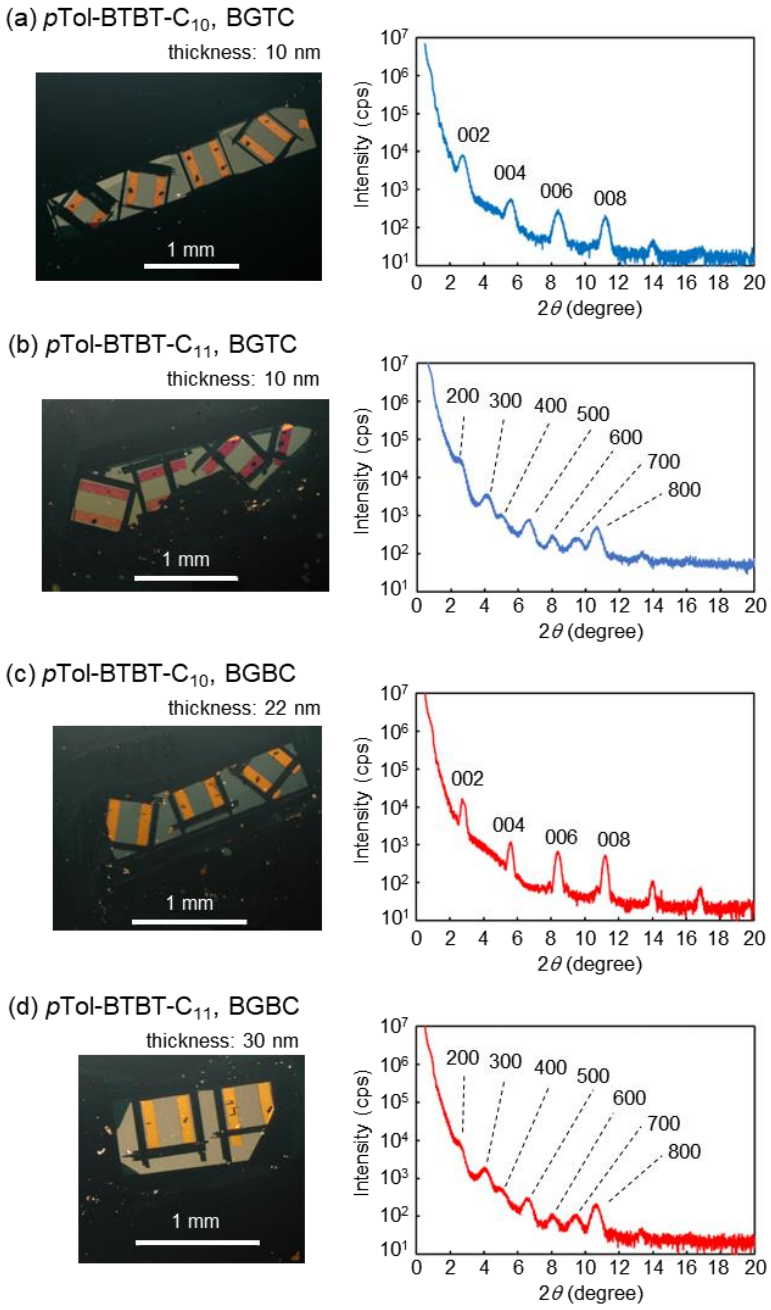

Figure S17. Out-of-plane XRD profiles of the single-crystal thin films used for (a) BGTC OFETs of *p*Tol-BTBT-C$_{10}$, and (b) BGTC OFETs of *p*Tol-BTBT-C$_{11}$, (c) BGBC OFETs of *p*Tol-BTBT-C$_{10}$, and (d) BGBC OFETs of *p*Tol-BTBT-C$_{11}$.

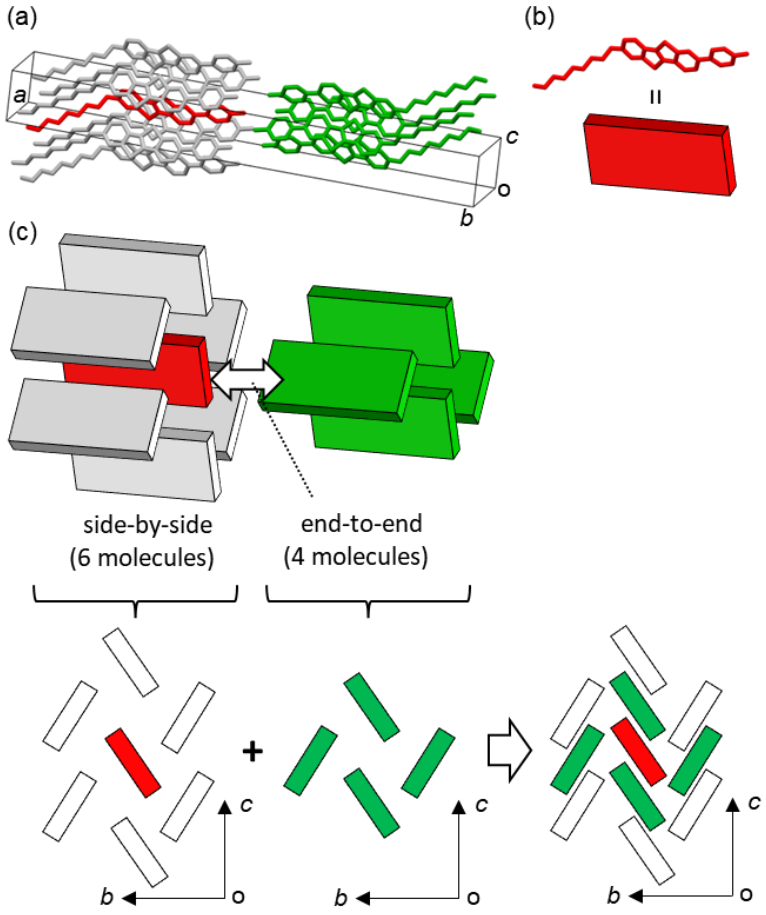

Figure S18. (a) The packing diagram of *p*Tol-BTBT-C_9 without hydrogen atoms. (b)(c) Schematic images of the intermolecular arrangement. Respective plates represent the *p*Tol-BTBT-C_9 molecule at the center (red), six neighboring *p*Tol-BTBT-C_9 molecules at the side-by-side contacts within the same layer (gray), and four neighboring *p*Tol-BTBT-C_9 molecules at the end-to-end contacts in the adjacent layer.

Table S2. Intermolecular interaction energies in *p*Tol-BTBT-C_n crystal packings.

chain length *n*	side-by-side interaction energy (kcal/mol)	end-to end interaction energy (kcal/mol)		
		alkyl-alkyl	tolyl-tolyl	alkyl-tolyl
9	−98.6	−2.73	−3.18	–
10	−103.3	–	–	−3.80
11	−106.3	−2.66	−3.21	-
12	−110.8	–	–	−3.89
13	−111.7	−2.94	−3.17	–
14	−118.2	–	–	−3.89

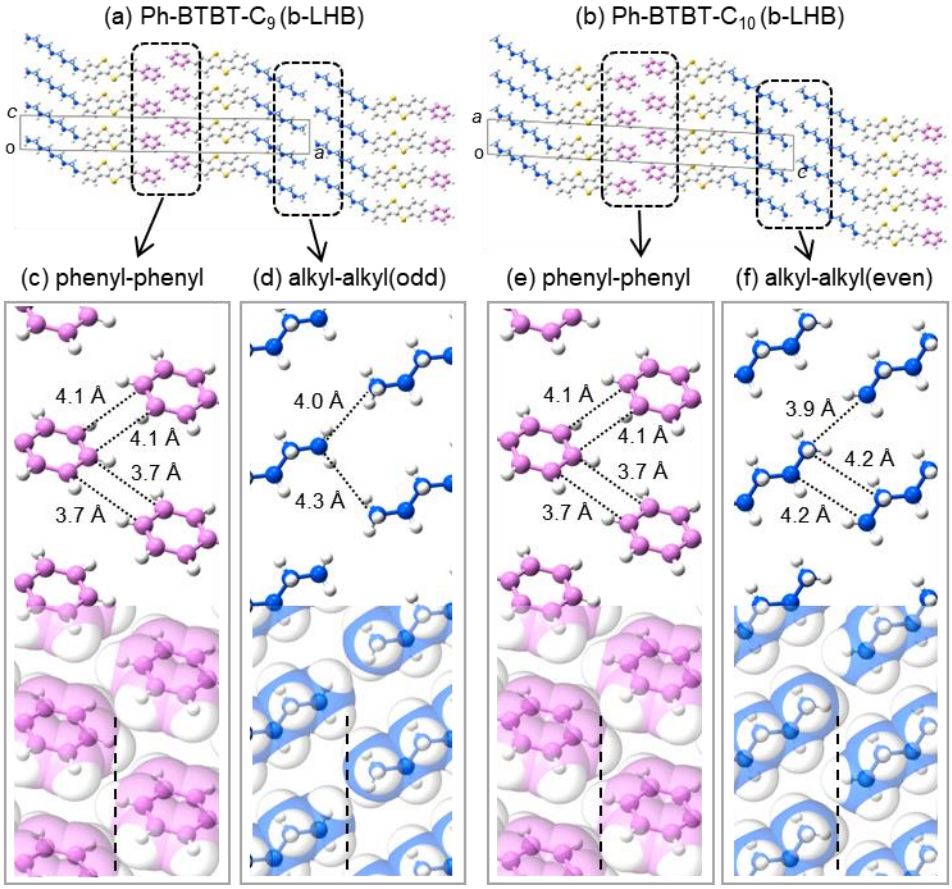

Figure S19. Packing diagrams of (a) Ph-BTBT-C_9 and (b) Ph-BTBT-C_{10} projected along the axis parallel to the π-stacking layers, and their interlayer arrangements around (c)(e) phenyl-phenyl, (d) alkyl-alkyl (odd), and (f) alkyl-alkyl (even) groups depicted by ball-and-stick views (top) and by space-filling views (bottom). The black dotted lines in the top show the connection of the pair of the carbon atom less than 4.5 Å in each interlayer. The black dashed lines in the bottom schematically show the layer-by-layer boundary.

Table S3. Miller indices using the lattice constant.

$n = 10$	$n = 11$
(1,1,1)	(0,1,1)
$(1,\bar{1},1)$	$(0,\bar{1},1)$
$(1,1,\bar{1})$	$(0,1,\bar{1})$
$(1,\bar{1},\bar{1})$	$(0,\bar{1},\bar{1})$
$(\bar{1},1,1)$	$(3,1,\bar{1})$
$(\bar{1},\bar{1},1)$	$(3,\bar{1},\bar{1})$
$(\bar{1},1,\bar{1})$	$(\bar{3},\bar{1},1)$
$(\bar{1},\bar{1},\bar{1})$	$(\bar{3},1,\bar{1})$

References for Methods

S1. Giannozzi, P., et al. QUANTUM ESPRESSO: a modular and open-source software project for quantum simulations of materials. *J. Phys. Condens. Matter* **21**, 395502 (2009).

S2. Giannozzi, P., et al. Advanced capabilities for materials modeling with QUANTUM ESPRESSO. *J. Phys. Condens. Matter* **29**, 465901 (2017).

S3. Frisch, M. J. et al., Gaussian 16, Revision A.03, Gaussian, Inc., Wallingford, CT, (2016).

S4. Grimme, S., Ehrlich, S., Goerigk, L. Effect of the damping function in dispersion corrected density functional theory. *J. Comp. Chem.* **32**, 1456-1465 (2011).

S5. Ransil, B. J. Studies in Molecular Structure. IV. Potential Curve for the Interaction of Two Helium Atoms in Single-Configuration LCAO MO SCF Approximation. *J. Chem. Phys.* **34**, 2109-2118 (1961).

S6. Boys, S. F., Bernardi, F. The calculation of small molecular interactions by the differences of separate total energies. Some procedures with reduced errors. *Mol. Phys.* **19**, 553-556 (1970).

S7. CrysAlisPro: Data Collection and Processing Software; Rigaku Corp..

S8. Rapid-AUTO: Data Collection and Processing Software; Rigaku Corp..

S9. Bourhis, L. J., Dolomanov, V. O., Gildea, R. J., Howard, J. A. K., Puschmann, H. The anatomy of a comprehensive constrained, restrained refinement program for the modern computing environment - Olex2 dissected *Acta Crystallogr., Sect. A: Found. Adv.* **71**, 59−75 (2015).

S10. Crystalstrucure 4.2.4: Crystal Structure Analysis Package; Rigaku Corp.

S11. Altomare, A., Cascarano, G., Giacovazzo, C., Guagliardi, A. Completion and refinement of crystal structures with SIR92. *J. Appl. Crystallogr.* **26**, 343-350 (1993).

S12. Burla, M. C., Caliandro, R., Camalli, M., Carrozzini, B., Cascarano, G. L., De Caro, L., Giacovazzo, C., Polidori, G., Spagna, R. SIR2004: an improved tool for crystal structure determination and refinement. *J. Appl. Crystallogr.* **38**, 381-388 (2005).

S13. Burla, M. C., Caliandro, R., Camalli, M., Carrozzini, B., Cascarano, G. L., De Caro, L., Giacovazzo, C., Polidori, G., Siliqi, D., Spagna, R. IL MILIONE: a suite of computer programs for crystal structure solution of proteins. *J. Appl. Crystallogr.* **40**, 609-613 (2007).

S14. Sheldrick, G. M., Crystal structure refinement with SHELXL. *Acta Crystallogr., Sect. C: Struct. Chem.* **71**, 3-8 (2015).

S15. Inoue, S., Minemawari, H., Tsutsumi, J., Chikamatsu, M., Yamada, T., Horiuchi, S., Tanaka, M., Kumai, R., Yoneya, M., Hasegawa, T. Effects of Substituted Alkyl Chain Length on Solution-Processable Layered Organic Semiconductor Crystals. *Chem. Mater.* **27**, 3809-3812 (2015).